The Dodge City Tornadoes on 24 May 2016: Understanding Cycloidal Marks in Surface Damage Tracks and Further Analysis of the Debris Cloud

ROGER M. WAKIMOTO,^a ZACHARY WIENHOFF,^b DYLAN REIF,^b HOWARD B. BLUESTEIN,^b AND DAVID C. LEWELLEN^c

(Manuscript received 1 October 2021, in final form 2 March 2022)

ABSTRACT: Mobile, polarimetric radar data were collected on a series of tornadoes that occurred near Dodge City, Kansas. A poststorm survey revealed a series of tornadic debris swaths in several dirt fields and high-resolution pictures of the tornado documented the visual characteristics of the tornado and the lofted debris cloud. The main rotational couplet associated with the tornado was identified in the single-Doppler velocities; however, no secondary rotational couplets were resolved in the low-level data performed during two consecutive volume scans. Numerical simulations have suggested that cycloidal damage swaths can result when debris is deposited as the low-level inflow turns upward in the corner region of the updraft annulus of the tornado core. This mechanism can dominate even when suction vortices are present in the simulations and can produce these swaths in the absence of these smaller-scale vortices. It is hypothesized that the observed cycloidal damage swaths were a result of the low-level inflow in the corner region of the tornado and not by the existence of suction vortices. Polarimetric data were combined with photographs of the tornado in order to document the lofted debris cloud and its relationship with the funnel. This analysis provided an opportunity to investigate whether recent findings describing the cross-correlation coefficient $\rho_{\rm hv}$ and differential reflectivity $Z_{\rm DR}$ signatures of the lofted debris cloud could be replicated. Regions of low $\rho_{\rm hv}$ at the periphery of the funnel cloud suggesting high debris loading and a column of negative $Z_{\rm DR}$ centered on the tornado believed to be produced by common debris alignment were noted.

SIGNIFICANCE STATEMENT: It is well known that some tornadoes produce smaller-scale vortices that rotate around the central axis of the main circulation. In addition, numerous aerial photographs have documented cycloidal debris marks within tornado damage tracks that traverse open fields. The prevailing theory shown in numerous text-books is that these marks are produced by these vortices. The current study suggests that this widely accepted model for producing these marks may be incorrect. It is suggested that these cycloidal marks are produced by the main tornado circulation and not by the smaller-scale vortices in this case.

KEYWORDS: Atmosphere; Extreme events; Severe storms; Tornadoes; Vortices; Convective storms; Radars/radar observations

1. Introduction

Fujita et al. (1970, 1976) and Fujita (1981) were among the first to use detailed damage surveys to reveal the finescale structure of tornado damage paths. In particular, they analyzed cycloidal and scalloping marks in open fields in the aftermath of tornadoes that had been traditionally attributed to scratch or gouge marks caused by large debris swirling within the low-level circulation of the vortex (e.g., Van Tassel 1955; Prosser 1964). The aerial and ground surveys performed

Denotes content that is immediately available upon publication as open access.

Wienhoff's current affiliation: Haag Engineering Co., Dallas, Texas. Reif's current affiliation: CoreLogic, Boulder, Colorado.

Corresponding author: Roger M. Wakimoto, wakimotoroger@gmail.com

by Fujita and his collaborators revealed that these cycloidal patterns were lines where debris had collected instead of scratch marks. Fujita et al. (1970, 1976) and Fujita (1981) hypothesized the existence of suction vortices, smaller-scale circulations within a tornado core that orbit around a central axis that were creating these lines of debris (see Fig. 15 in Fujita 1981). The existence of these suction vortices has been verified in numerical simulations (e.g., Lewellen et al. 2000), laboratory experiments (e.g., Church and Snow 1993), and in Doppler velocity measurements by mobile radars (e.g., Wurman 2002; Bluestein et al. 2018). In addition, numerous videos and photographs have visually documented these vortices.

From numerical simulations, Lewellen and Zimmerman (2008), Zimmerman (2010), and Zimmerman and Lewellen (2010) proposed an alternative mechanism for creating these cycloidal marks. They successfully recreated the debris lines in the shape of an arc form when a vortex traverses over a uniform surface of sand. However, they proposed that these lines were produced when low-level inflow turns sharply upward in the corner region in the updraft annulus of the

DOI: 10.1175/MWR-D-21-0262.1

^a Department of Atmospheric and Oceanic Sciences, University of California, Los Angeles, Los Angeles, California
^b School of Meteorology, University of Oklahoma, Norman, Oklahoma

^c Department of Mechanical and Aerospace Engineering, West Virginia University, Morgantown, West Virginia

tornado core. In addition, they noted that the tracks of the secondary vortices generally did not coincide with these lines of debris. These two competing models for explaining the cycloidal patterns documented during damage surveys have not been discussed in the literature since the Lewellen and Zimmerman (2008), Lewellen et al. (2008), Zimmerman (2010), and Zimmerman and Lewellen (2010) studies. The lack of progress on this topic is due to the difficulty of collecting mobile Doppler radar observations at low levels over a damage path when cycloidal marks were clearly documented during a poststorm survey. A study by Reiss et al. (2013) compared cycloidal marks in observed dust devils tracks with ones from numerical simulations, but the analysis of the formation mechanisms was limited by a lack of observations of the dust devils themselves. This paper presents an analysis of a tornado that developed near Dodge City, Kansas, on 24 May 2016. An aerial damage survey revealed a well-defined series of cycloidal damage swaths when the tornado traversed a dirt field during a time when mobile polarimetric radar data were recorded. These data combined with high-resolution photographs of the funnel and lofted debris cloud provide a unique opportunity to revisit the mechanism for creating these swath marks.

A second goal of this study is to elucidate the characteristics of lofted debris clouds. Analysis of data collected using mobile polarimetric radars has significantly improved our understanding of tornadoes. Polarimetric measurements can remotely distinguish the different types of hydrometeors but also identify characteristics of the debris cloud surrounding the condensation funnel (e.g., Ryzhkov et al. 2005; Bluestein et al. 2007, 2015; Kumjian and Ryzhkov 2008; Bodine et al. 2013, 2014; Snyder and Bluestein 2014; Kurdzo et al. 2015; Houser et al. 2016; Tanamachi et al. 2012; Van Den Broeke 2015; Wakimoto et al. 2015, 2016). The tornadic debris signature (TDS) was proposed by Ryzhkov et al. (2005) and is now a well-known indicator of debris lofted by a tornado. The TDS is typically associated with high radar reflectivity, low cross-correlation coefficient $\rho_{\rm hv}$, and low differential reflectivity Z_{DR} and is collocated with an intense rotational couplet. Defining precise threshold values in each of the categories has been challenging, as indicated by the results presented in past studies (e.g., Kumjian and Ryzhkov 2008; Bodine et al. 2013, 2014; Van Den Broeke and Jauernic 2014).

The lofted debris that surrounds the tornado can be as visually striking as the funnel cloud. The characteristics of the debris cloud are dependent on the tornadic wind speeds and the type of debris that is lofted (e.g., Lewellen et al. 2008). Although there have been numerous studies of the TDS documented by mobile radars and numerous photographs and videos of lofted debris, there are only a few studies that have combined polarimetric radar data with a photogrammetric analysis of the debris cloud. Bluestein et al. (2007) presented qualitative analyses of the TDS at low levels and compared it with a photograph of a tornado. Polarimetric

radar data were photogrammetrically merged with pictures of the 31 May 2013 El Reno, Oklahoma, tornado (Wakimoto et al. 2016). The tornado was large (~4-km damage path width) and resulted in eight fatalities. The TDS was approximately 2 km wide, but the debris cloud was poorly resolved in the photographs. Polarimetric measurements recorded by a mobile X-band radar were combined with photographs of the Dodge City, Kansas, tornado on 24 May 2016 to quantitatively document the evolving debris cloud (Wakimoto et al. 2018). The TDS and debris cloud were shown from early in the tornado's life cycle until the mature stage when the debris enveloped the funnel. Regions of high debris loading at low levels near the annulus of high radar reflectivity were documented. A column of negative Z_{DR} was centered on the tornado and is believed to be a result of common debris alignment. The radar and photogrammetric analysis in this paper provides an opportunity to replicate the findings presented by Wakimoto et al. (2018) on a different tornado.

Section 2 discusses the mobile radar platform used in this study, the aerial and ground survey, and the photogrammetric techniques used to analyze several photographs. A detailed analysis of the cycloidal damage marks and the radar analyses are presented in section 3. Polarimetric analyses combined with high-resolution photography of the funnel and lofted debris cloud are also shown. Section 4 discusses the two models for explaining the cycloidal marks and suggests which theory may explain the debris swaths noted in this study. A discussion and summary are presented in section 5.

2. RaXPol, damage survey, and photogrammetry

RaXPol is a mobile, X-band, polarimetric radar that was deployed in the present study. The antenna diameter is 2.4 m, the half-power beamwidth is 1°, and the wavelength is 3.1 cm. It is a rapidly scanning radar since the antenna can rotate up to a speed of 180° s⁻¹. The range gate spacing is 30 m, but the gates can be oversampled such that the spacing is 15 m. The nominal volume scan was completed in ~20 s and included elevation angles from 0° to 6° in 1° steps. For additional information about RaXPol, the reader is referred to Pazmany et al. (2013). There were two primary deployment sites of the radar (Fig. 1). RaXPol was located at site 1 from 2313 to 2346 UTC (UTC = central daylight time + 5 h) and site 2 from 2356 to 0006 UTC.

The damage tracks of the tornadoes were determined based on an aerial survey using a Cessna aircraft on 27 May 2016. A total of 10 tornadoes formed in the area west of Dodge City (Wakimoto et al. 2018). Nine of the tornado tracks are presented in Fig. 1. The EF ratings of the tornadoes are shown on the figure. Tornado 1 was scanned by RaXPol when it was deployed at site 1 and is the primary focus of this study. All of the tornadoes on this day occurred over rural areas, and the damage path primarily traversed either wheat or dirt fields. The uniformity of the dirt fields was similar to the lower boundary conditions in the numerical simulations of intense circulations by Lewellen and Zimmerman (2008) and Lewellen et al. (2008). As discussed by Wakimoto et al.

¹ Wienhoff et al. (2018) have examined radar data collected on this day and produced dual-Doppler analyses on several of the tornadoes.

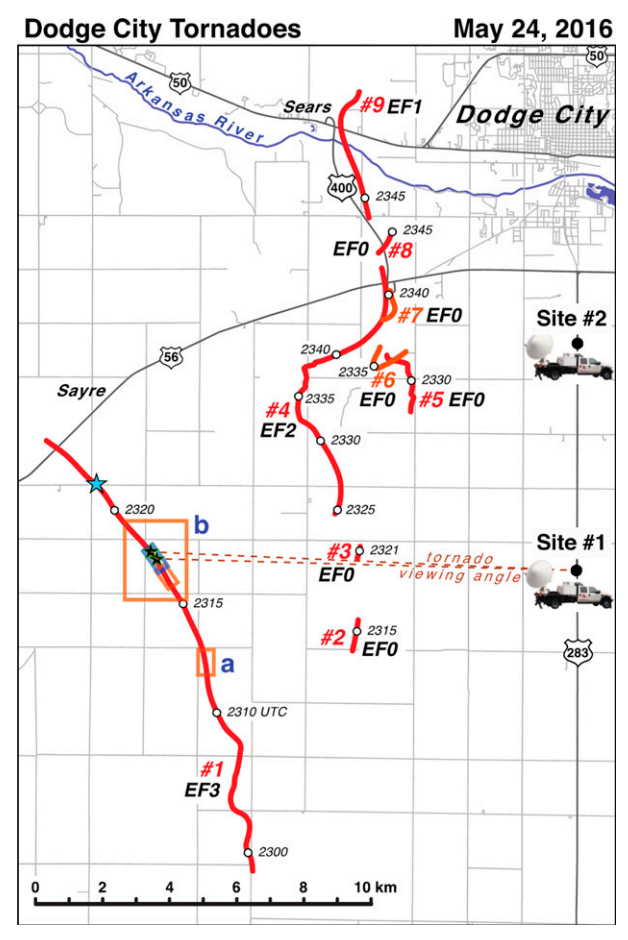


FIG. 1. A map illustrating the paths of the Dodge City tornadoes on 24 May 2016 as based on a damage survey. Red lines represent damage tracks of nine of the tornadoes that occurred on this day, with the locations of the tornado labeled at select times. The EF ratings are shown for each tornado. Black dots represent two deployment locations of the RaXPol mobile Doppler radar (an icon of the truck is plotted near each point). The blue star denotes the location where a house was destroyed (rated EF3). Black stars denote the locations of analyses presented in Figs. 10 and 11, below. The brown-outlined box labeled "a" is enlarged in Figs. 2, below. The brown-outlined box labeled "b" is enlarged in Figs. 4, 7, and 8, below. The smaller boxes enclosed in box b are also shown in Fig. 4, below.

(2018), there were several times when multiple tornadoes were simultaneously identified.

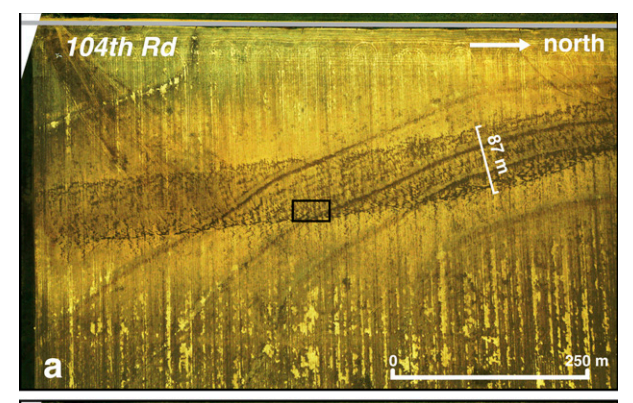
Photogrammetry is often used to quantitatively analyze pictures of tornadoes or cloud fields (e.g., Malkus 1952; Bluestein 1986; Wakimoto and Martner 1992; Zehnder et al. 2007; Wakimoto et al. 2012). Photogrammetry requires knowledge of both the camera focal length and the azimuth angles to ground targets identifiable on the horizon of the photograph. These two variables can subsequently be used to derive the effective focal length and the tilt angle of the camera, two key parameters that are required to calculate angular distances on an image. The final step is the construction of an azimuth- and elevation-angle grid that can be superimposed onto the

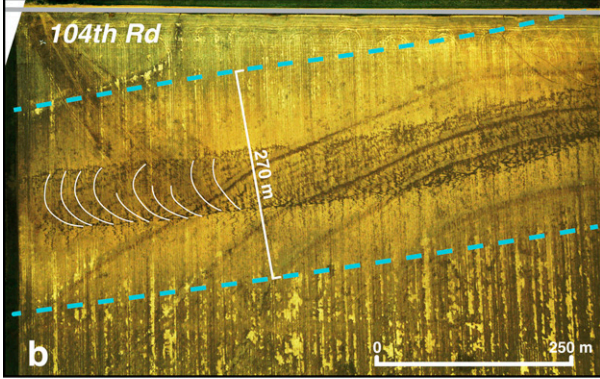
photograph. Abrams (1952) and Holle (1986) provide an overview of photogrammetry, the variables described above, and the calculations of angular distances on an image. A comparison of the azimuth angles of the targets with the calculated azimuth-angle grid suggest that the angle errors range between 0.1° and 0.2°, which range translates to 44–89 m at the distance of the tornado. The pictures were taken very close (2–3 m) to the radar antenna. Accordingly, the elevation- and azimuth-angle grid created using photogrammetry is equivalent to the radar scanning angles.

Vertical cross sections of the polarimetric variables at a constant range through the center of the rotational couplet were created using the raw data. The use of raw data rather than interpolated data produced a detailed analysis of the radar fields. These cross sections are along curved surfaces since a constant range is used. These analyses can be compared with the visual characteristics of the tornado and debris cloud. A small advection correction of the raw data was applied by shifting the radar data to account for the motion of the tornado (~9.5 m s⁻¹; however, the applied correction was only 7.9 m s⁻¹, which was the component of tornado motion in the plane of the photo) since the radar volume scans were completed in ~20 s. The correction varied with height since the near-ground and higher elevation angles were not scanned simultaneously. The polarimetric variables could contain statistical errors in areas of low signal-to-noise ratios such as the weak-echo column (WEC; Tanamachi et al. 2012) within the hook echo. It is possible that small shifts in the location of the vertical cross section could alter the analyses due to these errors. These errors were minimized by averaging $\rho_{\rm hv}$ and $Z_{\rm DR}$ over five consecutive range gates (a 75 m average in the present case). Additional information about this averaging can be found in Wakimoto et al. (2018). To remove errors in $Z_{\rm DR}$, the horizontal and vertical channels of radar reflectivity were calibrated by collecting data in stratiform precipitation where $Z_{\rm DR}$ should be near zero. Offset corrections were applied to the dataset presented in this study.

3. Damage track and radar analysis of tornado 1

Tornado 1 created a damage path that was ~15 km long and was rated EF3 on the enhanced Fujita scale based on the destruction of a house in which one person was injured (denoted by the blue star in Fig. 1). Fortunately, the rest of the tornado track avoided structures but left behind welldefined damage markings in the wheat and dirt fields. A prominent feature of the tornado track when it passed over the dirt fields was the clear definition of the core width estimated to be ~87 m in Fig. 2a. This core measure approximately defines the location of the tornado's corner flow where the near-surface flow turns upward. Reiss et al. (2013) noted that the vortex core at the surface was denoted by regions where sand was deposited. The track shown in this figure was also one of the best-documented examples in the literature of the locations where dirt was either removed or deposited within and beyond the tornado core in response to strong convergent flow into the circulation. A larger area outside the core where surface dirt has been scoured by the tornado is





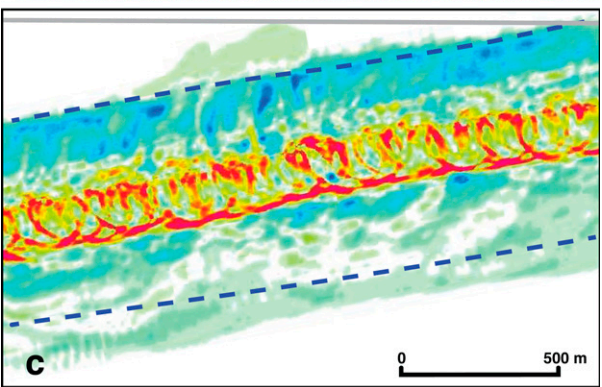


FIG. 2. The damage path of tornado 1: (a) aerial photograph of the damage, (b) aerial photograph of the damage path with dashed blue lines indicating the width where the dirt has been scoured by the tornado, and (c) a numerical simulation of a damage path associated with a translating high-swirl tornado from Lewellen and Zimmerman (2008). Yellow and red colors represent regions where dirt has been deposited, and green and blue areas represent regions where dirt has been removed from the ground. The dashed blue lines from (b) have been transposed onto (c). The black-outlined box drawn on (a) is enlarged in Fig. 3, below. The width of the tornado core is shown in (a). Several swath marks have been highlighted by the thin white lines in (b). The box shown in this figure has been rotated and is shown by the label "a" in Fig. 1. The gray line at the top of the figure is a road.

highlighted by the light-blue dashed lines (Fig. 2b). The width of this area is approximately 3 times the width of the core. The aircraft altitude was ~900 m above ground level (AGL) when the photograph shown in Figs. 2a and 2b was taken. It

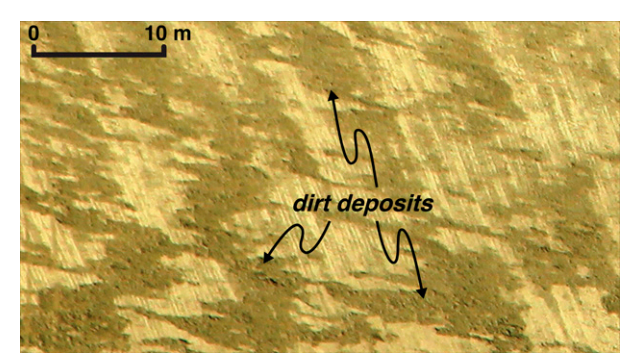


FIG. 3. Enlargement of the box shown in Fig. 2a revealing that the dark-brown areas are regions where dirt has been deposited by the tornado. The light-brown areas denote where dirt has been removed.

was not possible to determine what the marks in the photographs represented from this altitude. Accordingly, the aircraft descended to ~120 m AGL to document the finescale features of the tornado track. An enlarged image (Fig. 3) reveals that the dark- or light-brown areas are regions where dirt has been deposited or removed, respectively. Small ridges of dirt, separated by ~0.3 m, produced by a cultivator are oriented approximately perpendicular to the tornado track (Figs. 2 and 3). Cycloidal or scalloping marks as documented by Fujita et al. (1976) are suggested at several locations along the track. Several of these marks have been highlighted by the white lines (Fig. 2b).

RaXPol was in the process of parking and leveling the truck at site 1 during the time that the tornado traversed the field shown in Fig. 2. Fortunately, tornado 1 passed over several dirt fields after the radar began collecting data (Fig. 4). The tornado produced continuous, cycloidal swaths marks in the dirt fields for a distance of ~2 km (Fig. 4). The approximate diameter of the marks was consistent with the estimated size of the funnel shown at two locations in the figure. The tornado was located 12-13 km from the radar site during this time. The poststorm aerial survey revealed numerous cycloidal or swath marks as the tornado traversed the dirt fields (Fig. 5a). The location of these marks has been precisely plotted on Fig. 4. Similar to the image shown in Fig. 2, the large region of dirt removed outside the main tornado circulation is apparent (Fig. 5b). The width of the area of scoured dirt is the same as in Fig. 2b suggesting that the kinematic structure of the tornado was in approximately steady state during this time. The location of the center of the rotational couplet based on a low-level scan from RaXPol is shown by the red circle (Fig. 5b).

Swath marks were also documented in an adjacent dirt field (Figs. 4 and 6). The marks are highlighted by the white lines in Fig. 6b. Simulations performed by Lewellen and Zimmerman (2008) suggest that the vortex translation produces a tilt in the circulation and the debris cloud. The latter leads to asymmetric deposits of the lofted debris to the right and rearward relative to the tornado motion aloft, which could explain the location of the swath marks shown in Fig. 6.

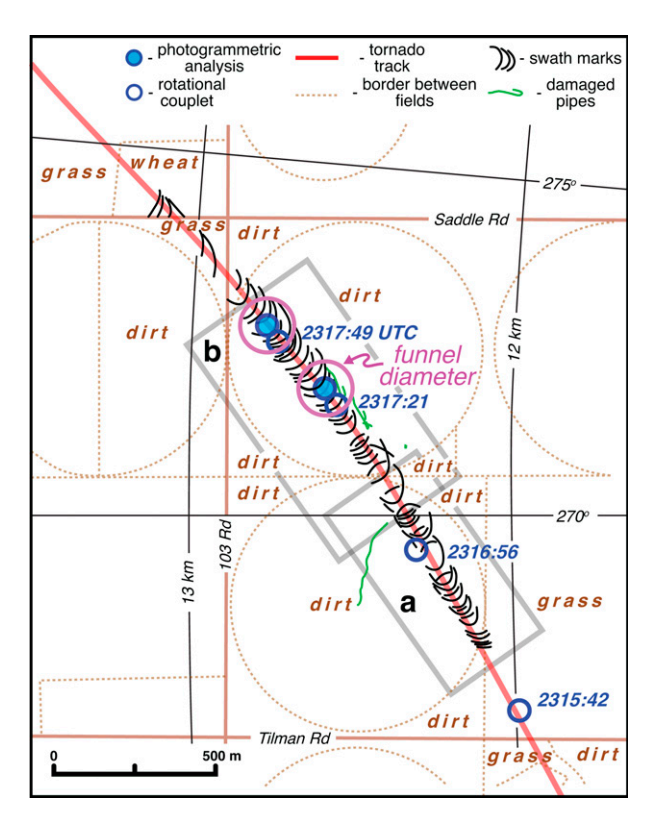


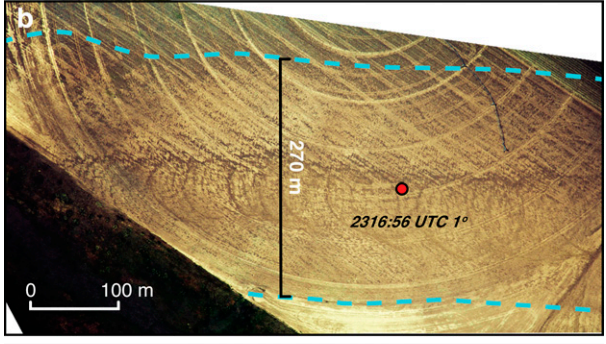
FIG. 4. Analysis of cycloidal marks (black lines) in dirt fields traversed by tornado 1 based on an aerial survey. The red line denotes the tornado track. The location of the rotational couplet is shown by the blue circles. The magenta circles represent the width of the tornado funnel. The azimuth and range from RaXPol are indicated by the thin, black lines. Damaged irrigation pipes are shown by the green lines. The characteristics of the fields (dirt, wheat, or grass) are labeled on the figure. Locations where photogrammetric analyses of the tornado photographs were performed are shown by the solid blue circles. The box shown in this figure is shown by the label "b" in Fig. 1. The smaller gray-outlined boxes labeled "a" and "b" in this plot are also plotted in Fig. 1 and are enlarged in Figs. 5 and 6, respectively, as shown below.

The yellow circles represent the width of the funnel cloud at low levels based on photogrammetric measurements to be discussed later in this section. The first complete radar scanning volumes collected by RaXPol were at 2317:21 and 2317:49 UTC. The location of the rotational couplet during these times are denoted by the blue circles in Fig. 6.

This is believed to be the first time that mobile radar measurements were collected on a tornado when a series of well-defined swath/scalloping marks were confirmed by a damage survey and photographs/videos of the funnel were recorded.

Low-level scans (0°) at 2317:21 and 2317:49 UTC superimposed onto the damage track are presented in Figs. 7 and 8, respectively. The dimension of the lofted debris cloud depicted in photographs presented later in this section is denoted by the blue circle. A weak-echo hole surrounded by higher reflectivity (e.g., Fujita 1981; Wurman et al. 1996; Wakimoto et al. 1996; Wurman and Gill 2000; Dowell et al. 2005) is apparent at both times (Figs. 7a and 8a) although is better defined at 2317:21





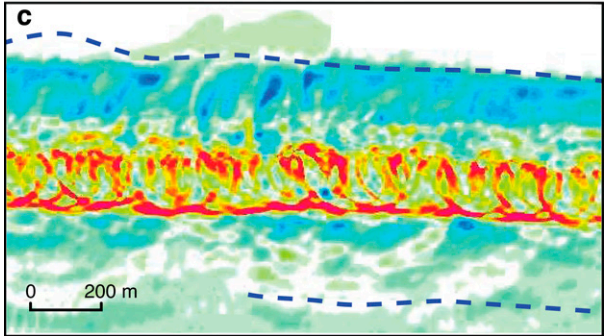
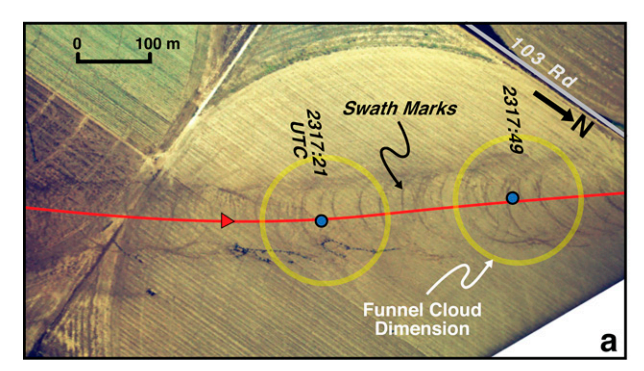


FIG. 5. The damage path of tornado 1: (a) aerial photograph of the damage, (b) aerial photograph of the damage path with dashed blue lines indicating the width where the dirt has been scoured by the tornado, and (c) a numerical simulation of a damage path associated with a translating high-swirl tornado from Lewellen and Zimmerman (2008). Yellow and red colors represent regions where dirt has been deposited, and green and blue areas represent regions where dirt has been removed from the ground. The dashed blue lines from (b) have been transposed onto (c). The area shown in this figure is highlighted by the gray-outlined box labeled "a" in Fig. 4. The red circle denotes the location of the rotational couplet.

UTC. The TDS is shown by the quasi-circular region of relatively low $\rho_{\rm hv}$ (Figs. 7c and 8c) and $Z_{\rm DR}$ (Figs. 7d and 8d) and is consistent with the lofted debris outlined by the blue circle. The rotational couplet is apparent in the single-Doppler velocity fields (Figs. 7b and 8b) and the slight asymmetry in the approaching and receding velocity can be partially explained by the tornado's translation. Tornado 1 was estimated to be translating at 9.5 m s⁻¹ to the northwest (see Fig. 1). This motion would add or subtract ~5.3 m s⁻¹ to the magnitude of the approaching or receding speeds, respectively.



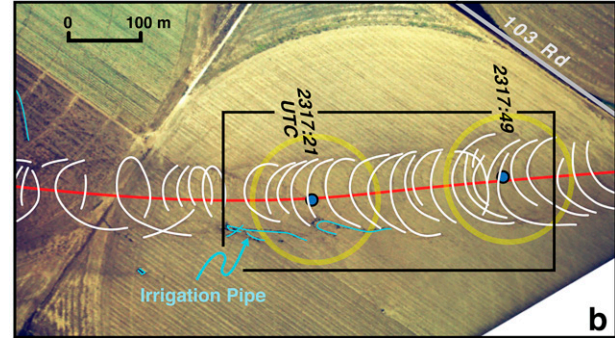


FIG. 6. Aerial photograph of the damage path of tornado 1. The red line represents the center of the tornado track. The yellow circles represent the funnel width at low levels. The locations of the rotational couplet at two times are shown by the blue circles. The swath marks are highlighted by the white lines in (b). The blue lines in (b) denote damaged irrigation pipes. The area shown in the figure is highlighted by the gray-outlined box labeled "b" in Fig. 4.

Although the rotational couplet associated with tornado 1 is apparent in Figs. 7b and 8b, there are no smaller rotational signatures that suggest the presence of suction vortices for either time. Velocity data at 1° (~218 m AGL) and 2° (~436 m AGL) elevation angles (not shown) also did not resolve smaller scale circulations. High spectral width (not shown) was identified along the radial between the approaching and receding velocities as would be expected. No other regions of high spectral width could be identified that might indicate the presence of smaller-scale shear zones (i.e., suction vortices). It is possible that the absence of suction vortices in the radar data is due to azimuthal resolution (0.8° or 175 m at the distance of the tornado). However, it would be expected that there would be a suggestion of their presence in light of the large number of swath marks surveyed in this case and the series of elevation angle scans recorded in each volume.

Numerous photographs of tornado 1 were taken from the RaXPol radar site. High-spatial-resolution data collected at 2317:21–2317:38 and 2317:49–2318:04 UTC of radar reflectivity, single-Doppler velocity, $\rho_{\rm hv}$, and $Z_{\rm DR}$ at the distance of the tornado were plotted on the images at 2317:27 and 2317:56 UTC, respectively, using the photogrammetrically derived elevation- and azimuth-angle grids. This technique allowed for a comparison of the radar variables with the visual characteristics of the tornado (e.g., Wakimoto et al. 2015, 2018).

The width of the funnel cloud was estimated to be 175 m at ~250 m AGL. The funnel diameter was plotted on Figs. 4 and 6 and suggests that it is slightly larger than the tornado core width defined by the cycloidal debris swaths. An enlargement of suction swaths is presented in Fig. 9. The black circles denote two estimates of the tornado core diameter based on the surface debris swaths. The core in Fig. 9 appears to widen from 100 m (~2317:20 UTC) to 120 m (~2317:40 UTC) between the two analysis times shown in Figs. 10 and 11, respectively. There is no quantitative change in the visible width of the cloud funnel between these times (cf. Figs. 10a and 11a) providing additional evidence that the funnel dimension is not an accurate indicator of the width of the tornado core (e.g., Golden and Purcell 1978; Bluestein et al. 2004). The magnitudes of the approaching and receding velocities

depicted in Figs. 7b and 8b are greater than 50 and 70 m s⁻¹, respectively. As previously mentioned, the asymmetry was partially attributable to the translation of the tornado. The average peak rotational velocity of the tornado was \sim 65 m s⁻¹.

The lofted debris cloud is \sim 1 km in diameter (Figs. 10a and 11a), which is larger than the area of scoured dirt (270 m wide) depicted in the aerial photographs because of centrifuging of the lofted debris (e.g., Dowell et al. 2005; Lewellen et al. 2008). The visual characteristics of the funnel cloud and lofted debris cloud are similar to the numerical simulations presented by Lewellen et al. (2008, see their Fig. 1). Their simulated tornado was translating at 15 m s⁻¹, the debris was composed of 1-mm-diameter sand particles, and the core velocity was 74.4 m s⁻¹. The core velocity of tornado 1 was \sim 65 m s⁻¹, and it was translating at 9.5 m s⁻¹.

The images of tornado 1 presented in Figs. 10 and 11 along with other photographs taken of the tornado at this time (not shown) did not suggest the existence of suction vortices. Numerous videos of tornado 1 recorded by storm chasers were reviewed (not shown). Some of the chasers' locations were less than 2 km from the funnel at the same time of the analyses shown in this paper. No multiple vortices were identified in these videos. The funnel is laminar in appearance and suggests the presence of a single circulation, which is consistent with the Doppler velocity signature (Figs. 7b and 8b). However, a laminar structure does not preclude the existence of smaller-scale vortices hidden within the funnel. Videos taken by chasers near the beginning of the tornado track (not shown) did reveal secondary vortices. This location was 9-10 km south southeast of the analysis region shown in Fig. 4. These small-scale vortices did not produce debris swaths according to the aerial survey of the damage. Interestingly, there is no study in the literature that has documented a series of scalloping or looping marks in surface damage patterns (e.g., Fujita et al. 1976) during a period when suction vortices were visually confirmed with videos or photographs. This absence is remarkable in light of the numerous images and videos of tornadoes in recent years.

A WEC within the hook echo (<5 dBZ) centered on the funnel cloud is apparent (Figs. 10b and 11b). The vertical

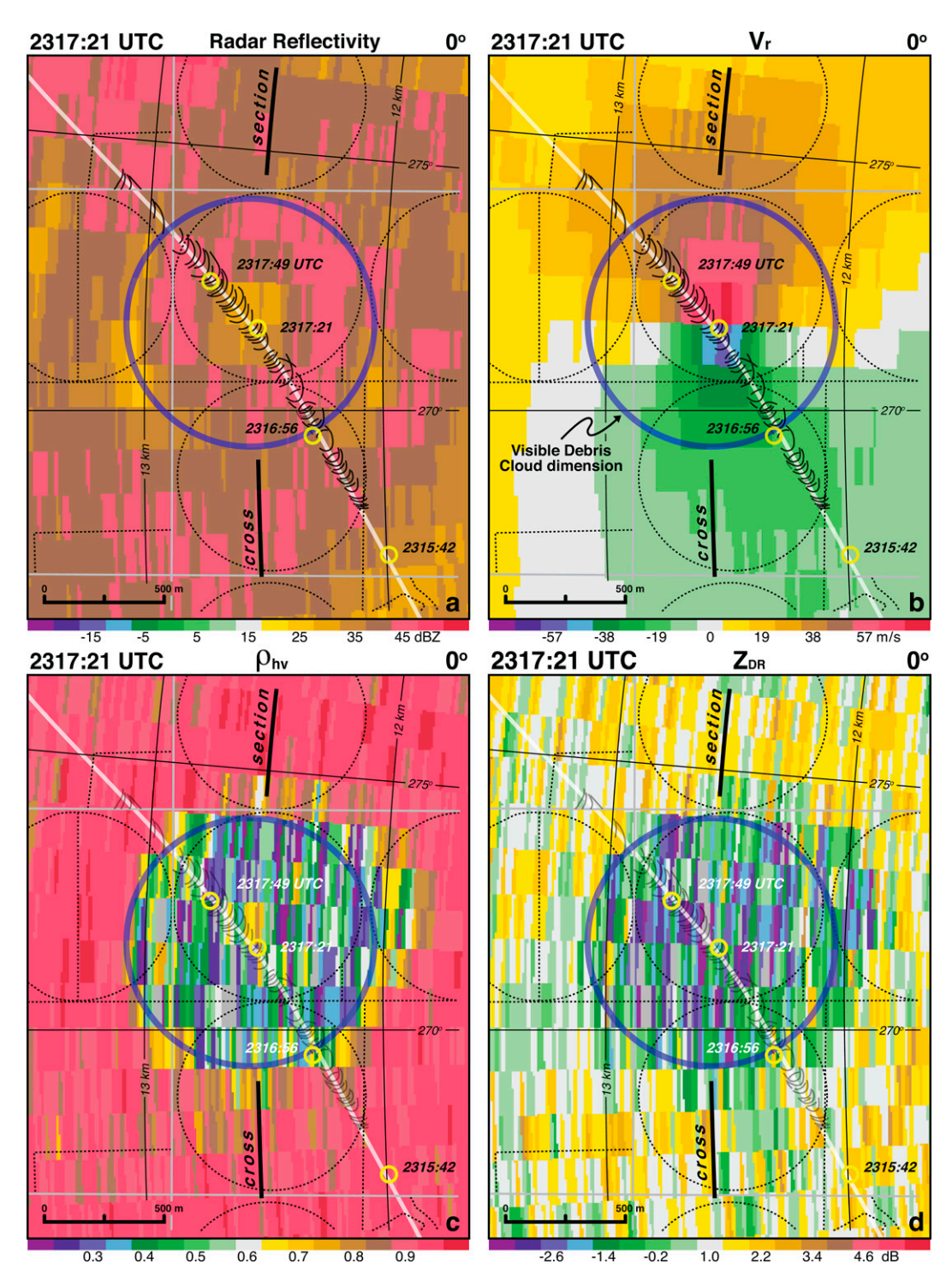


Fig. 7. Scan from RaXPol at 0° elevation angle at 2317:21 UTC: (a) radar reflectivity, (b) single-Doppler velocities Vr, (c) cross-correlation coefficient ρ_{hv} , and (d) differential radar reflectivity Z_{DR} . The range and azimuth angle grid is shown by the thin black lines. Cycloidal debris swaths are shown by the partial black circles. Dotted lines separate fields with different ground characteristics (see Fig. 4). Yellow circles represent the subjective locations of the center of the rotational couplet. The blue circle represents the location of the lofted debris cloud depicted in Fig. 10, below. Gray lines denote roads. The thick black line represents the location of the cross section shown in Fig. 10. The area enclosed is as in Fig. 4 and is also shown in Fig. 1.

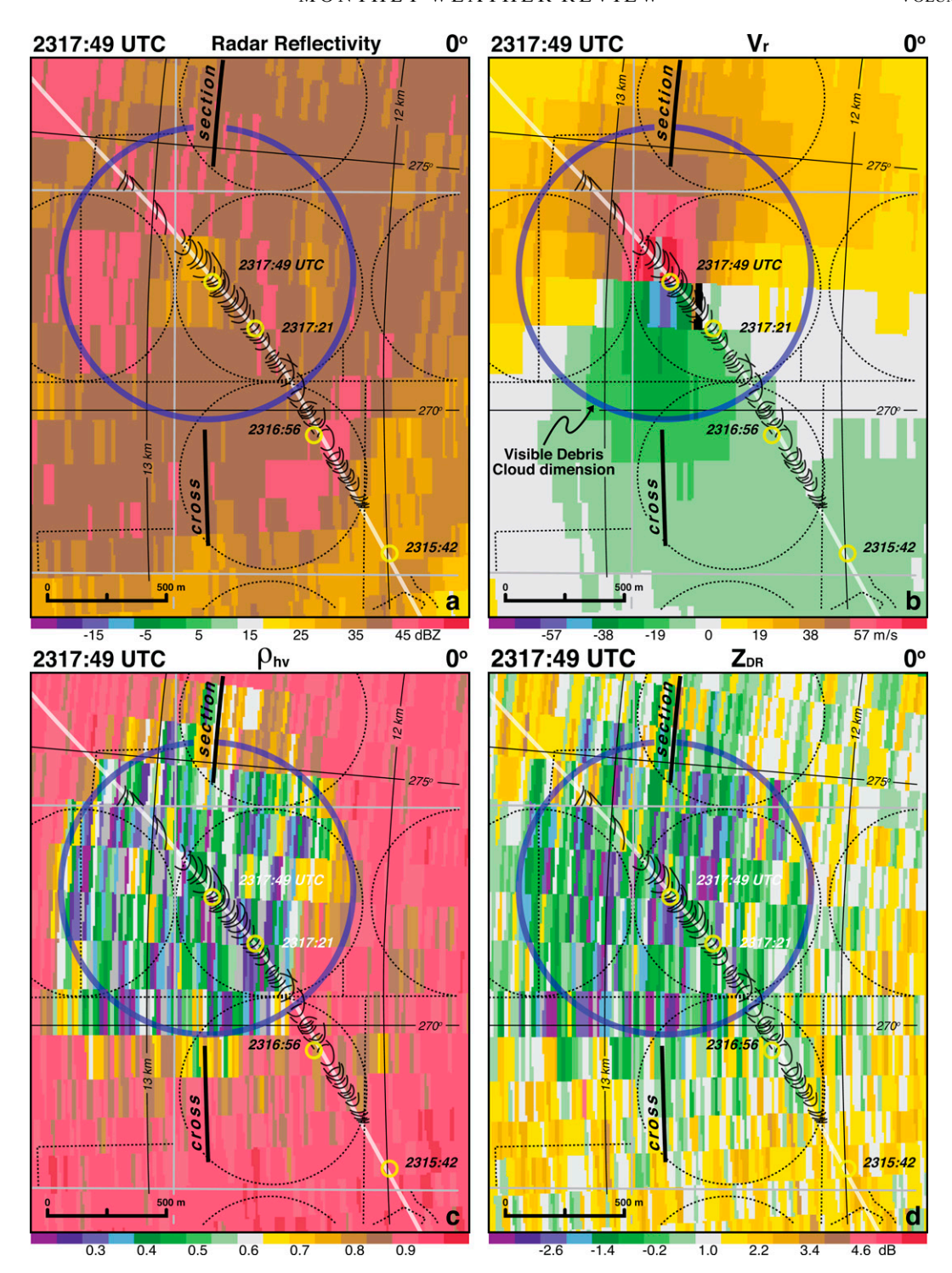
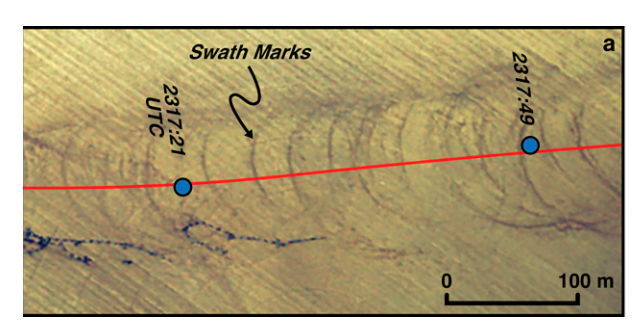


FIG. 8. As in Fig. 7, but at 2317:49 UTC. The blue circle represents the location of the lofted debris cloud depicted in Fig. 11, below. The thick black line represents the location of the cross section shown in Fig. 11.

profile in ρ_{hv} (Figs. 10d,f) reveals a trough approximately centered on the funnel cloud. However, there are also two areas of low ρ_{hv} and relatively high radar reflectivity surrounding the funnel cloud at low levels (white arrows). Low ρ_{hv} and higher echo intensity suggest that these are regions of high

debris loading or areas of larger debris sizes present in low concentrations outside the funnel cloud. This feature was also noted by Wakimoto et al. (2018) for another tornado on this day providing additional evidence that this may be a characteristic debris signature. The extension of the low $\rho_{\rm hv}$ features



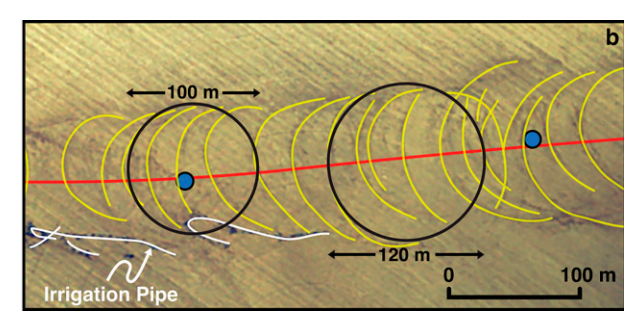


FIG. 9. (a) Enlargement of the suction swath marks created by tornado 1. (b) Yellow lines highlight the locations of the suction swath marks. The black circles represent the approximate tornado core width at two locations along the track. The red line denotes the center of the tornado track. Blue circles denote the location of the rotational couplet. The area shown in the figure is enclosed by the black-outlined box in Fig. 6b.

just outside the funnel extends to higher levels at the next volume time (Figs. 11d,f) and is an indication of debris being lofted to greater heights. The cross section of differential reflectivity (Fig. 10e) reveals negative $Z_{\rm DR}$ within the WEC and low ρ_{hv} trough. Wakimoto et al. (2018) hypothesized that the negative Z_{DR} could be a result of common debris alignment (Ryzhkov et al. 2005; Bluestein et al. 2007). They proposed that wheat stems were lofted by the tornado when it passed over wheatfields at an earlier time. Wheat stems are not expected to be reflective or could be present in low concentrations, which would explain the negative Z_{DR} column within the WEC. Common debris alignment in lofted debris composed of leaves within tornadoes has also been simulated by Cheong et al. (2017) and Umeyama et al. (2018). Bodine et al. (2014) proposed that given the wide range of scatterer characteristics within a resolution volume, some degree of common scatterer alignment could produce negative $Z_{\rm DR}$ even when ρ_{hv} is low. The negative Z_{DR} column is still prominent in the next analysis time (Fig. 11e).

4. Comparison with numerical simulated damage tracks

Lewellen and Zimmerman (2008), Lewellen et al. (2008), Zimmerman (2010), and Zimmerman and Lewellen (2010) reproduced surface debris swaths using a high-resolution large-eddy simulation (LES) model. The vertical and horizontal grid spacing were 1 m near the surface and 4 or 5 m in the central corner flow, respectively. The simulations were performed with sand (1-mm diameter). They noted that, unless there were dramatic changes in parameters that determine how the sand was "picked up," the changes in the surface track appearance were modest. The present study is one of the first opportunities to examine the Lewellen and Zimmerman (2008) and Zimmerman and Lewellen (2010) hypothesis for creating debris swaths. This comparison with tornado 1 is relevant since the observational analysis suggests that suction vortices may not have been present; yet, well-defined cycloidal marks over a significant segment of the damage path were documented. An example of surface marks produced by a high-swirl tornado translating at ~15 m s⁻¹ is presented in Figs. 2c and 5c (Lewellen and Zimmerman 2008). The plot of the simulated track was adjusted so that the tornado core

diameter approximately matched the width of tornado 1 in the figure (the simulated tornado was larger than tornado 1 based on the length scale). The adjustment allowed for a relative comparison of the observed and simulated tornadoes.

Prominent cycloidal marks similar to those documented by Fujita et al. (1970, 1976) and Fujita (1981) are apparent in Figs. 2c and 5c. In contrast to the suction vortex hypothesis, the surface marks in their simulations result from debris accumulating when low-level inflow turns sharply upward in the corner region in the updraft annulus of the tornado core. Debris is subsequently deposited in lines that closely resemble cycloidal marks. Moreover, the Lewellen and Zimmerman (2008) and Zimmerman and Lewellen (2010) studies revealed that in the simulated tracks of high-swirl tornadoes the cycloidal marks did not coincide with the paths of multiple secondary vortices when they were present. Further, cycloidal debris lines were also found in many simulations with only a single tornadic vortex. An axisymmetric vortex would naturally be expected to produce a deposition track symmetric along the direction of travel. But the simulated tornadoes, like their real counterparts, included fluctuations in the air and debris flows, breaking the axisymmetry of the debris deposition pattern at any instant. Convoluted over time this produced the "cycloidal marks" of the tracks. Contributions to these fluctuations were many, including: turbulence within the corner flow of the vortex (including secondary vortices when present), variations in debris flow being swept in radially (e.g., due to surface inflow rolls), wandering of the debris ring gathered by the updraft annulus due to its own inertia/instability, and vortex translation.

The dashed blue lines in Fig. 2b denote the area where dirt has been removed by the tornado. These dashed lines have been transposed onto Fig. 2c. The relative area where debris is scoured closely resembles the observations shown in Figs. 2a and 2b. The simulation by Lewellen and Zimmerman (2008) has also been plotted in Fig. 5c. The numerical plot of debris swaths resembles the observed tornado marks and the region where dirt has been scoured is also consistent with the simulations.

The numerical simulations can be interpreted using four dimensionless ratios (e.g., Lewellen et al. 2000, 2008; Zimmerman 2010):

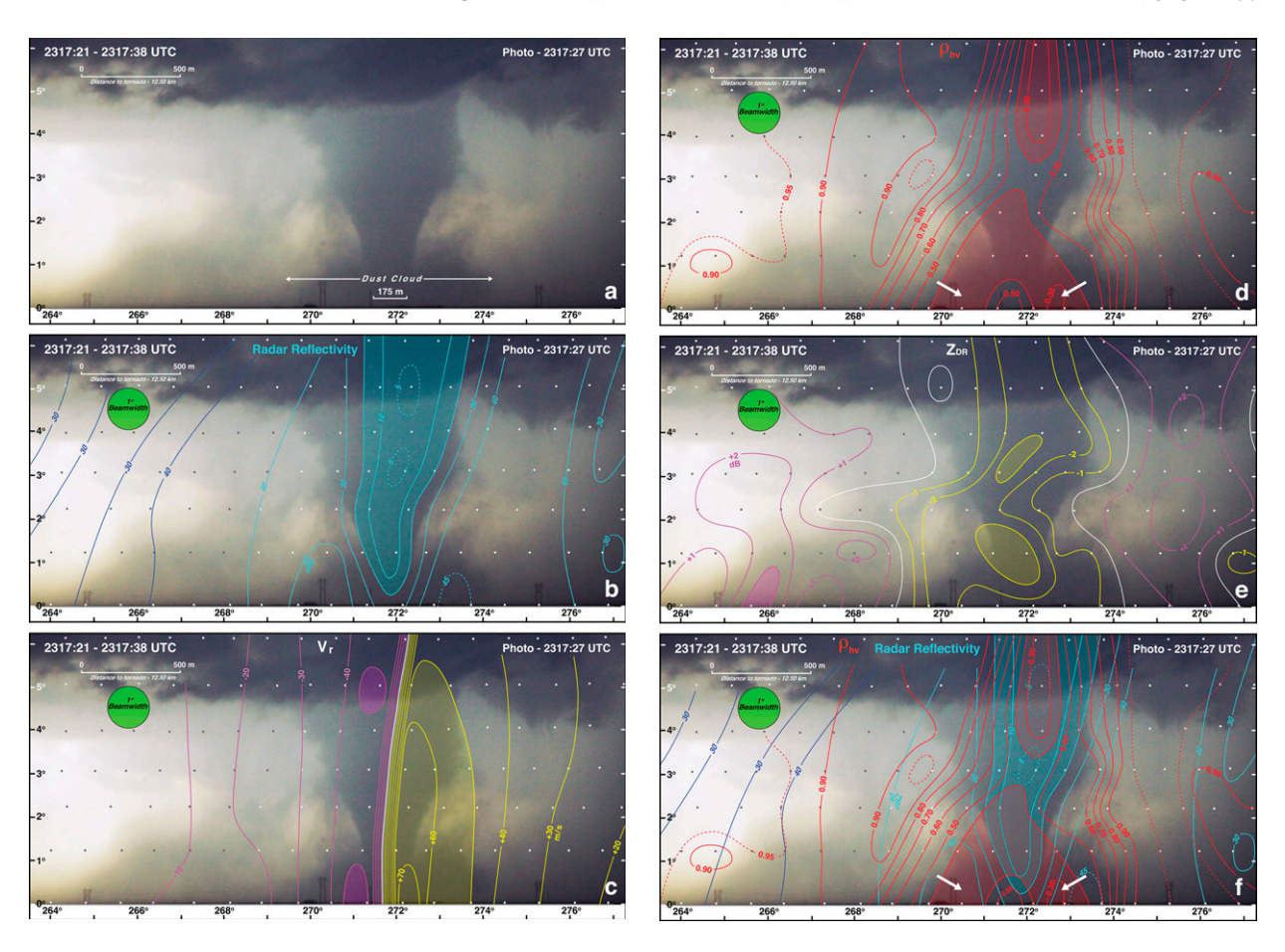


FIG. 10. (a) Photograph of Dodge City tornado 1 at 2317:27 UTC. The radar volume scan is 2317:21–2317:38 UTC. (b) Radar reflectivity (dBZ). Values <20 dBZ are shaded light blue. (c) Ground-relative single-Doppler velocities (m s⁻¹). Magenta and yellow lines are isopleths of approaching and receding single-Doppler velocities, respectively (magnitudes > 50 m s⁻¹ are shaded). (d) Cross-correlation coefficient ρ_{hv} . Values < 0.40 are shaded red. (e) Differential reflectivity Z_{DR} (dB). Yellow and magenta lines are isopleths of negative and positive Z_{DR} , respectively; Z_{DR} > 3 dB are shaded magenta, and Z_{DR} < -3 dB are shaded yellow. (f) Radar reflectivity and ρ_{hv} . The green circle represents the 1° beamwidth of the radar. The scales labeled on the photographs are valid at the distance to the center of the tornado. The small dots represent the raw data points from RaXPol. The location of the tornado at this time is shown in Figs. 1, 4, and 7. The white arrows in (d) and (f) denote regions of higher radar reflectivity and low ρ_{hv} .

$$S_c \equiv R_c \Gamma_{\infty}^2 / Y,\tag{1}$$

$$A_v \equiv V_c/w_t,\tag{2}$$

$$A_a \equiv V_c^2/(gR_c)$$
, and (3)

$$A_t \equiv U_{\text{trans}}/V_c,$$
 (4)

where V_c and R_c are the peak core swirl velocity and radial scales aloft above the corner flow, respectively; Γ_∞ is the far-field angular momentum aloft and outside the core; Y is the depleted angular momentum flux (the total flux of the local flow variable $\Gamma_\infty - \Gamma$) through the surface-corner-core flow; g is the gravitational acceleration; U_{trans} is the vortex translation velocity; and w_t is the terminal speed of the debris in freefall. Lewellen et al. (2000) defines $R_c = \Gamma_\infty/V_c$. Ratio S_c is the corner flow swirl ratio and roughly categorizes tornado type.

Ratio A_v parameterizes the amount of debris slip relative to the airflow. Increasing A_v lessens the maximum potential amount of slip. Ratio A_a measures the importance of a characteristic radial acceleration relative to gravity, and A_t measures the relative importance of the vortex translation speed. Several of these variables can be estimated using the analyses presented in Figs. 10c and 11c as follows: $V_c \sim 50$ m s⁻¹, $\Gamma_\infty \sim 19\,000$ m² s⁻¹, and $R_c \sim 380$ m. As previously mentioned, $U_{\rm trans} \sim 9.5$ m s⁻¹. There will be a range of debris involved in forming the surveyed damage track. A good approximation for w_b used in many of the numerical simulations, was 5.7 m s⁻¹. These approximations lead to estimates of three of the four dimensionless parameters: $A_v \sim 8.7$, $A_a \sim 0.67$, and $A_t \sim 0.19$.

The corner flow swirl ratio S_c cannot be directly computed but there are inferences based on the observed tornado structure. The shape of the observed debris cloud and the comparison with numerical simulations suggest a medium to high

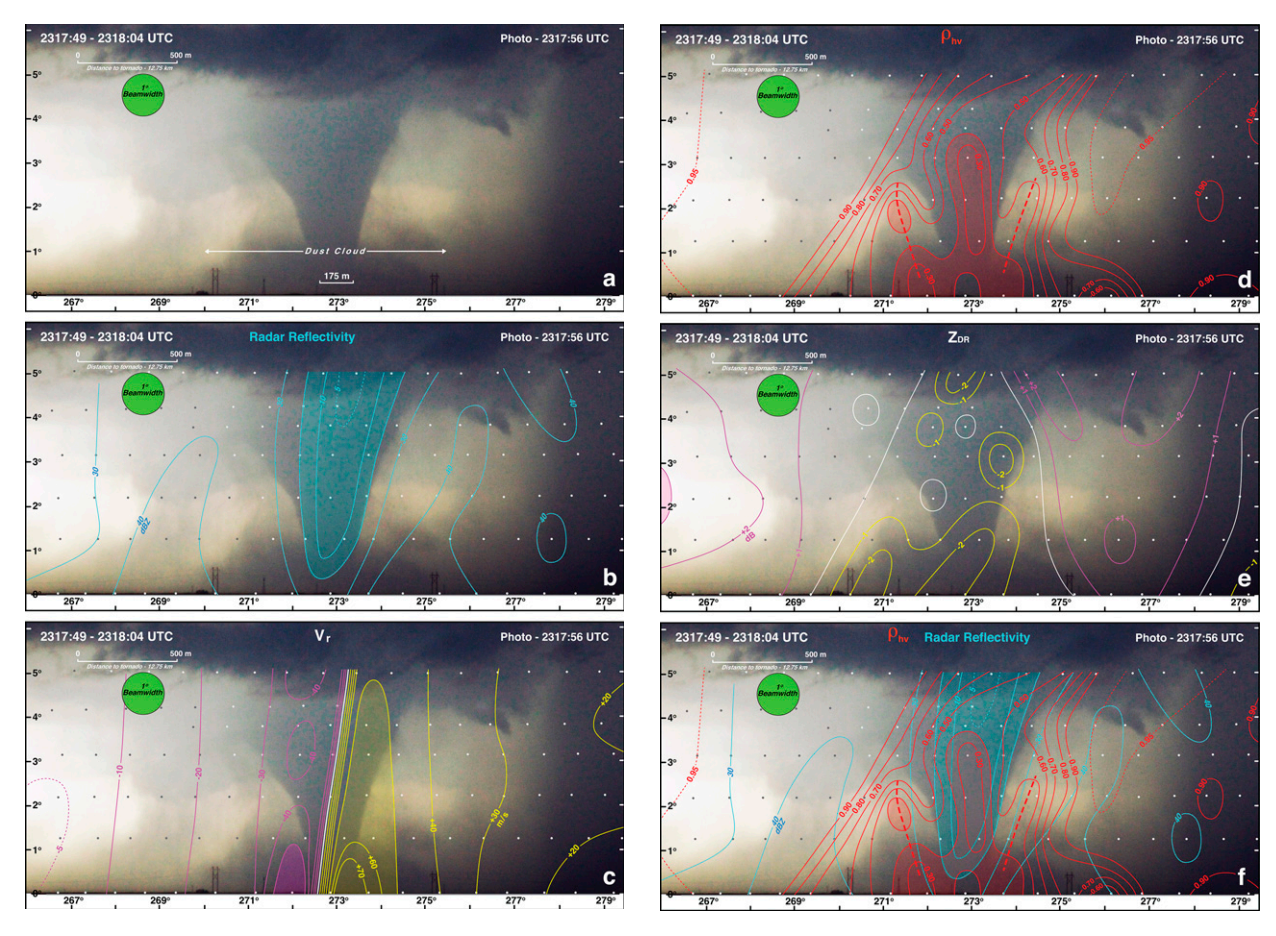


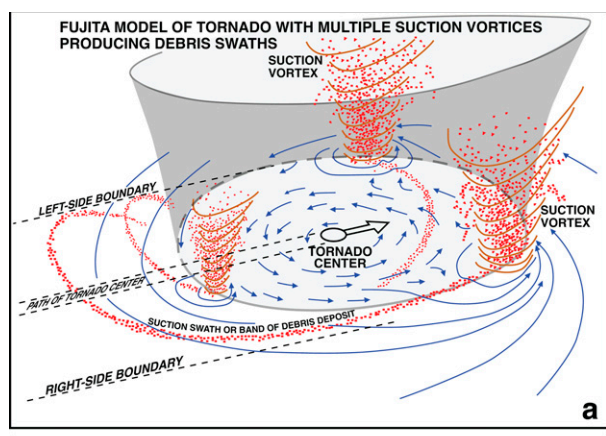
Fig. 11. As in Fig. 10, but at 2317:56 UTC. The radar volume scan is 2317:49–2318:04 UTC. The location of the tornado at this time is shown in Figs. 1, 4, and 8.

swirl corner flow (i.e., $S_c > 2$). The radial scale of the swath marks (Fig. 9) is ~60 m, less than the radius of maximum winds, which ranges from 100 to 150 m (Figs. 10c and 11c). The difference in the radii and the apparent absence of strong secondary vortices suggests that the observed tornado is closer to a medium rather than high swirl. Accordingly, a good estimate of S_c would be between 2 and 8.

The simulation shown in Fig. 5c is associated with following parameters: $A_v = 12.2$, $A_a = 2.39$, $A_t = 0.21$, and $S_c = 12.4$. The values of A_a and S_c in the simulations are higher than the estimates associated with the Dodge City tornado. The suite of simulations produced by Zimmerman (2010) and Zimmerman and Lewellen (2010) where A_a and S_c are closer to the values estimated from the Dodge City tornado (not shown) resulted in debris swaths that are consistent with those shown in Figs. 2 and 5. None matched the Dodge City tornado in all four parameters; the simulation case shown in Fig. 5 was chosen for illustration because the color figure showed the swath marks most clearly. The most prominent difference is reducing the length scale of the cycloidal marks relative to the core radial scale aloft R_c , which brings them in closer agreement to the observed marks produced by the Dodge City tornado. The comparisons of the observed

cycloidal debris marks with the numerical simulations over a range of parameter space strongly suggest that debris swaths were associated with the updraft annulus at the surface rather than the secondary vortices. Indeed, many of the simulated cases did not produce these vortices even though prominent cycloidal debris marks were produced.

A comparison of the two models for creating debris swath marks is presented in Fig. 12. The Fujita model (Fig. 12a) that proposes that these marks are produced by suction vortices has been accepted since the 1970s and has been referenced in numerous articles and textbooks. The model proposed by Lewellen and Zimmerman (2008) and Zimmerman and Lewellen (2010) suggests that these marks are a result of deposited debris when low-level inflow turns upward in the corner region in the updraft annulus of the tornado core (Fig. 12b). No suction vortices are plotted on the latter figure since their presence is not required to produce cycloidal marks in this model. The results suggest that the model proposed in Fig. 12b may be the primary mechanism for creating the swaths produced by tornado 1. Mobile radar data collecting higher-spatial-resolution data while simultaneously taking videos/photographs when similar markings are produced by a tornado would provide a more definitive answer.



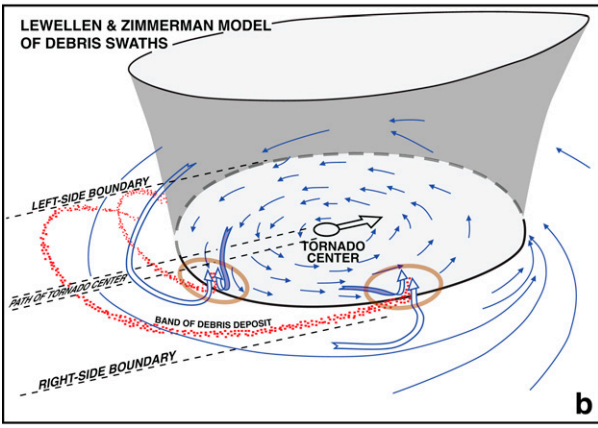


FIG. 12. Schematic models for producing cycloidal debris marks. (a) The model proposed by Fujita hypothesized that suction vortices revolving around the center axis create these debris swaths. (b) The Lewellen and Zimmerman model proposes that these marks result from debris that is deposited when low-level inflow turns sharply upward in the corner region in the updraft annulus of the tornado core (locations are highlighted by brown ellipses). The mechanism in (b) does not require secondary vortices, which may or may not be present in a given case.

The numerical simulations suggest a mechanism for producing debris swaths in open fields that are not attributable to suction vortices. This hypothesis, however, does not imply that these smaller-scale circulations have a negligible impact on the observed damage to houses and buildings. The strong wind speeds in these vortices (e.g., Wurman et al. 2014) could result in intense damage to structures that lie within their path. In addition, we cannot conclude at this point that all cycloidal debris swaths are produced by the mechanism discussed in this paper or that the presence of secondary vortices never impacts cycloidal marks.

5. Discussion and summary

A detailed aerial mapping of the damage path of a tornado near Dodge City was presented. Prominent debris swaths that have been previously documented in the literature were present in several dirt fields. Clearly shown was the much larger area located at the periphery of the tornado core where dirt was scoured from the field. A series of high-resolution pictures of the tornado documented the visual characteristics of the tornado and lofted debris cloud. The funnel cloud appeared laminar during the time that the debris swaths were being created and there was no visual evidence of the existence of suction vortices when the tornado traversed these fields. A primary rotational couplet associated with the tornado was identified in single-Doppler velocities recorded by a mobile radar; however, no secondary rotational couplets were apparent in the scans.

The analysis of the Dodge City tornado provided an opportunity to compare the observations with the numerical simulations presented by Lewellen and Zimmerman (2008), Lewellen et al. (2008), and Zimmerman and Lewellen (2010). The intense circulations generated in their simulations traversed dirt fields and produced lofted debris clouds that share many of the characteristics of the Dodge City tornado. The swaths produced at the surface were a result of deposited debris when low-level inflow turns upward in the corner region in the updraft annulus of the tornado core. A fraction of the debris swept into this narrow region of strong horizontal convergence is unable to follow the large acceleration of the airflow from the radial direction into the vertical and is left behind. This can occur even when the debris terminal velocity is small enough that the debris could have been lofted if it had remained within the annular updraft. These cycloidal debris lines can form even when only a single tornadic vortex is simulated. The results presented in this paper provide the first observational evidence that suggests that the cycloidal debris swaths associated with the Dodge City tornado may have been produced by this alternative mechanism. Indeed, radar observations suggest that the tornado was characterized by a single vortex. Numerical simulations suggest that even when secondary vortices exist, they may not be the causal mechanism for creating debris swaths documented during aerial surveys. Future studies will require high temporal and spatial resolution radar data, photograph and video documentation, and detailed damage surveys of tornado tracks. These data will help to determine the validity of the two models presented in Fig. 12.

In the future, it is recommended that these lines be referred to as cycloidal debris swaths or debris swaths rather than suction vortex swaths/marks based on the observations presented in this paper. In addition, the term suction vortex should also be reconsidered. Fujita (1981) proposed that these small-scale vortices were "sucking" debris into the cycloidal lines observed in the aftermath of tornadoes, which does not appear to be the case. Secondary vortices would be the preferred terminology.

Polarimetric radar data were combined with high-resolution photographs of the tornado to document the lofted debris cloud and its relationship with the funnel. This analysis provided an opportunity to investigate whether the findings presented by Wakimoto et al. (2018) were replicated for a different tornado on this day. A column of low $\rho_{\rm hv}$ contained primarily within the WEC was noted. There were two regions of low $\rho_{\rm hv}$ at low level located at the periphery of the funnel

cloud that were attributed to high debris loading. A column of negative $Z_{\rm DR}$ was centered on the tornado and is believed to be produced by common debris alignment. These observations suggest that these polarimetric signatures may be characteristic of tornadoes traversing open terrain where dirt, grass, and wheat fields predominate.

Acknowledgments. This work was supported by NSF Grants AGS-1560945, 1947146, and 082131. The latter is an NSF MRI grant for RaXPol. The authors are grateful to Boon Leng Cheong, Danny Feland, John Meier, Dale Sexton, David Bodine, and Tian Yu at the Advanced Radar Research Center at the University of Oklahoma for housing and maintaining RaXPol.

Data availability statement. RaXPol data are available online upon request to H. Bluestein at the School of Meteorology, University of Oklahoma, Norman.

REFERENCES

- Abrams, T., 1952: *The Manual of Photogrammetry*. George Banta Publishing, 876 pp.
- Bluestein, H. B., 1986: Visual aspects of the flanking line in severe thunderstorms. *Mon. Wea. Rev.*, **114**, 788–795, https://doi.org/10.1175/1520-0493(1986)114<0788:VAOTFL>2.0.CO;2.
- —, C. C. Weiss, and A. L. Pazmany, 2004: The vertical structure of a tornado near Happy, Texas, on 5 May 2002: High-resolution, mobile, W-band, Doppler radar observations. *Mon. Wea. Rev.*, 132, 2325–2337, https://doi.org/10.1175/1520-0493(2004)132<2325:TVSOAT>2.0.CO;2.
- —, M. M. French, R. L. Tanamachi, S. Frasier, K. Hardwick, F. Junyent, and A. L. Pazmany, 2007: Close-range observations of tornadoes in supercells made with dual-polarization, X-band, mobile, Doppler radar. *Mon. Wea. Rev.*, 135, 1522–1543, https://doi.org/10.1175/MWR3349.1.
- —, J. C. Snyder, and J. B. Houser, 2015: A multiscale overview of the El Reno, Oklahoma, tornadic supercell of 31 May 2013. Wea. Forecasting, 30, 525–552, https://doi.org/10.1175/ WAF-D-14-00152.1.
- —, K. J. Thiem, J. C. Snyder, and J. B. Houser, 2018: The multiple-vortex structure of the El Reno, Oklahoma, tornado on 31 May 2013. *Mon. Wea. Rev.*, **146**, 2483–2502, https://doi. org/10.1175/MWR-D-18-0073.1.
- Bodine, D. J., M. R. Kumjian, R. D. Palmer, P. L. Heinselman, and A. V. Ryzhkov, 2013: Tornado damage estimation using polarimetric radar. *Wea. Forecasting*, 28, 139–158, https://doi. org/10.1175/WAF-D-11-00158.1.
- ——, R. D. Palmer, and G. Zhang, 2014: Dual-wavelength polarimetric radar analyses of tornadic debris signatures. *J. Appl. Meteor. Climatol.*, **53**, 242–261, https://doi.org/10.1175/JAMC-D-13-0189.1.
- Cheong, B. L., D. J. Bodine, C. J. Fulton, S. M. Torres, T. Maruyama, and R. D. Palmer, 2017: SimRadar: A polarimetric radar time series simulator for tornadic debris studies. *IEEE Trans. Geosci. Remote Sens.*, 55, 2858–2870, https://doi.org/10.1109/TGRS.2017.2655363.
- Church, C. R., and J. T. Snow, 1993: Laboratory models of tornadoes. The Tornado: Its Structure, Dynamics, Prediction, and Hazards, Geophys. Monogr., Vol. 79, Amer. Geophys. Union, 277–295.

- Dowell, D. C., C. R. Alexander, J. M. Wurman, and L. J. Wicker, 2005: Centrifuging of hydrometeors and debris in tornadoes: Radar-reflectivity patterns and wind-measurement errors. *Mon. Wea. Rev.*, 133, 1501–1524, https://doi.org/10.1175/MWR2934.1.
- Fujita, T. T., 1981: Tornadoes and downbursts in the context of generalized planetary scales. J. Atmos. Sci., 38, 1511–1534, https://doi.org/10.1175/1520-0469(1981)038<1511:TADITC> 2.0.CO:2.
- —, D. L. Bradbury, and C. F. Van Thullenar, 1970: Palm Sunday tornadoes of April 11, 1965. *Mon. Wea. Rev.*, 98, 29–69, https://doi.org/10.1175/1520-0493(1970)098<0029:PSTOA>2.3.CO;2.
- —, G. S. Forbes, and T. A. Umenhofer, 1976: Close-up view of 20 March 1976 tornadoes: Sinking cloud tops to suction vortices. Weatherwise, 29, 116–145, https://doi.org/10.1080/00431672.1976. 10544142.
- Golden, J. H., and D. Purcell, 1978: Life cycle of the Union City, Oklahoma, tornado and comparison with waterspouts. *Mon. Wea. Rev.*, **106**, 3–11, https://doi.org/10.1175/1520-0493(1978) 106<0003;LCOTUC>2.0.CO:2.
- Holle, R. L., 1986: Photogrammetry of thunderstorms. *Thunderstorms: A Social and Technological Documentary*, 2nd ed. E. Kessler, Ed., Vol. 3, University of Oklahoma, 77–98.
- Houser, J. L., H. B. Bluestein, and J. C. Snyder, 2016: A finescale radar examination of the tornadic debris signature and weak echo reflectivity band associated with a large, violent tornado. *Mon. Wea. Rev.*, 144, 4101–4130, https://doi.org/10.1175/ MWR-D-15-0408.1.
- Kumjian, M. R., and A. V. Ryzhkov, 2008: Polarimetric signatures in supercell thunderstorms. J. Appl. Meteor. Climatol., 47, 1940–1961, https://doi.org/10.1175/2007JAMC1874.1.
- Kurdzo, J. M., D. J. Bodine, B. L. Cheong, and R. D. Palmer, 2015: High-temporal resolution polarimetric X-band Doppler radar observations of the 20 May 2013 Moore, Oklahoma, tornado. *Mon. Wea. Rev.*, 143, 2711–2735, https://doi.org/10. 1175/MWR-D-14-00357.1.
- Lewellen, D. C., and M. I. Zimmerman, 2008: Using simulated tornado surface marks to help decipher near-ground wind fields. 24th Conf. on Severe Local Storms, Savannah, GA, Amer. Meteor. Soc., 8B1, https://ams.confex.com/ams/24SLS/ webprogram/Paper141749.html.
- —, W. S. Lewellen, and J. Xia, 2000: The influence of a local swirl ratio on tornado intensification near the surface. J. Atmos. Sci., 57, 527–544, https://doi.org/10.1175/1520-0469 (2000)057<0527:TIOALS>2.0.CO;2.
- —, B. Gong, and W. S. Lewellen, 2008: Effects of finescale debris on near-surface tornado dynamics. *J. Atmos. Sci.*, 65, 3247–3262, https://doi.org/10.1175/2008JAS2686.1.
- Malkus, J., 1952: The slopes of cumulus clouds in relation to external wind shear. *Quart. J. Roy. Meteor. Soc.*, 78, 530–542, https://doi.org/10.1002/qj.49707833804.
- Pazmany, A. L., J. B. Mead, H. B. Bluestein, J. C. Snyder, and J. B. Houser, 2013: A mobile rapid-scanning X-band polarimetric (RaXPol) Doppler radar system. J. Atmos. Oceanic Technol., 30, 1398–1413, https://doi.org/10.1175/JTECH-D-12-00166.1.
- Prosser, N. E., 1964: Aerial photographs of a tornado path in Nebraska, May 5, 1964. Mon. Wea. Rev., 92, 593–598, https:// doi.org/10.1175/1520-0493(1964)092<0593:APOATP>2.3.CO;2.
- Reiss, D., M. I. Zimmerman, and D. C. Lewellen, 2013: Formation of cycloidal dust devil tracks by redeposition of coarse sands in southern Peru: Implications for Mars. *Earth Planet. Sci. Lett.*, 383, 7–15, https://doi.org/10.1016/j.epsl.2013.09.033.

- Ryzhkov, A., T. Schuur, D. W. Burgess, and D. S. Zrnić, 2005: Polarimetric tornado detection. J. Appl. Meteor., 44, 557–570, https://doi.org/10.1175/JAM2235.1.
- Snyder, J. C., and H. B. Bluestein, 2014: Some considerations for the use of high-resolution mobile radar data in tornado intensity determination. *Wea. Forecasting*, 29, 799–827, https://doi. org/10.1175/WAF-D-14-00026.1.
- Tanamachi, R. L., H. B. Bluestein, J. B. Houser, S. J. Frasier, and K. M. Hardwick, 2012: Mobile, X-band, polarimetric Doppler radar observations of the 4 May 2007 Greensburg, Kansas, tornadic supercell. *Mon. Wea. Rev.*, 140, 2103–2125, https:// doi.org/10.1175/MWR-D-11-00142.1.
- Umeyama, A., B. L. Cheong, S. Torres, and D. Bodine, 2018: Orientation analysis of simulated tornadic debris. *J. Atmos. Oceanic Technol.*, 35, 993–1010, https://doi.org/10.1175/JTECH-D-17-0140.1.
- Van Den Broeke, M. S., 2015: Polarimetric tornadic debris signature variability and debris fallout signatures. J. Appl. Meteor. Climatol., 54, 2389–2405, https://doi.org/10.1175/JAMC-D-15-0077.1.
- —, and S. T. Jauernic, 2014: Spatial and temporal characteristics of polarimetric tornadic debris signatures. *J. Appl. Meteor. Climatol.*, **53**, 2217–2231, https://doi.org/10.1175/JAMC-D-14-0094.1.
- Van Tassel, E. L., 1955: The North Platte Valley tornado outbreak of June 27, 1955. Mon. Wea. Rev., 83, 255–264, https://doi.org/ 10.1175/1520-0493(1955)083<0255:TNPVTO>2.0.CO;2.
- Wakimoto, R. M., and B. E. Martner, 1992: Observations of a Colorado tornado. Part II: Combined photogrammetric and Doppler radar analysis. *Mon. Wea. Rev.*, 120, 522–543, https://doi.org/10.1175/1520-0493(1992)120<0522:OOACTP> 2.0.CO:2.
- —, W.-C. Lee, H. B. Bluestein, C.-H. Liu, and P. H. Hildebrand, 1996: ELDORA observations during VORTEX 95. *Bull. Amer. Meteor. Soc.*, 77, 1465–1481, https://doi.org/10.1175/1520-0477(1996)077<1465:EODV>2.0.CO;2.
- ——, P. Stauffer, and W.-C. Lee, 2012: Finescale structure of the LaGrange, Wyoming, tornado during VORTEX2: GBVTD and photogrammetric analysis. *Mon. Wea. Rev.*, **140**, 3397–3418, https://doi.org/10.1175/MWR-D-12-00036.1.
- —, N. T. Atkins, K. M. Butler, H. B. Bluestein, K. Thiem, J. Snyder, and J. Houser, 2015: Photogrammetric analysis of the

- 2013 El Reno tornado combined with mobile X-band polarimetric radar data. *Mon. Wea. Rev.*, **143**, 2657–2683, https://doi.org/10.1175/MWR-D-15-0034.1.
- —, and Coauthors, 2016: Aerial damage survey of the 2013 El Reno tornado combined with mobile radar data. *Mon. Wea. Rev.*, 144, 1749–1776, https://doi.org/10.1175/MWR-D-15-0367.1.
- —, Z. Wienhoff, H. B. Bluestein, and D. Reif, 2018: The Dodge City tornadoes on 24 May 2016: Damage survey, photogrammetric analysis combined with mobile polarimetric radar data. *Mon. Wea. Rev.*, **146**, 3735–3771, https://doi.org/10.1175/ MWR-D-18-0125.1.
- Wienhoff, Z. B., H. B. Bluestein, L. J. Wicker, J. C. Snyder, A. Shapiro, C. K. Potvin, J. B. Houser, and D. W. Reif, 2018: Applications of a spatially variable advection correction technique for temporal correction of dual-Doppler analyses of tornadic supercells. *Mon. Wea. Rev.*, 146, 2949–2971, https://doi.org/10.1175/MWR-D-17-0360.1.
- Wurman, J., 2002: The multiple-vortex structure of a tornado. Wea. Forecasting, 17, 473–505, https://doi.org/10.1175/1520-0434(2002)017<0473:TMVSOA>2.0.CO;2.
- —, and S. Gill, 2000: Finescale radar observations of the Dimmitt, Texas (2 June 1995), tornado. *Mon. Wea. Rev.*, **128**, 2135–2164, https://doi.org/10.1175/1520-0493(2000)128<2135: FROOTD>2.0.CO;2.
- —, J. M. Straka, and E. N. Rasmussen, 1996: Fine-scale Doppler radar observations of tornadoes. *Science*, 272, 1774–1777, https://doi.org/10.1126/science.272.5269.1774.
- —, K. Kosiba, P. Robinson, and T. Marshall, 2014: The role of multiple-vortex tornado structure in causing storm researcher fatalities. *Bull. Amer. Meteor. Soc.*, 95, 31–45, https://doi.org/ 10.1175/BAMS-D-13-00221.1.
- Zehnder, J. A., J. Hu, and A. Razdan, 2007: A stereo photogrammetric technique applied to orographic convection. *Mon. Wea. Rev.*, 135, 2265–2277, https://doi.org/10.1175/MWR3401.1.
- Zimmerman, M. I., 2010: Correlating simulated surface marks with near-surface tornado structure. Ph.D. dissertation 3206, Eberly College of Arts and Sciences, West Virginia University, 144 pp., https://researchrepository.wvu.edu/etd/3206/.
- —, and D. C. Lewellen, 2010: Taxonomy and analysis of simulated tornado surface marks. 25th Conf. on Severe Local Storms, Denver, CO, Amer. Meteor. Soc., P10.5, https://ams.confex.com/ams/pdfpapers/175683.pdf.